International Conference on Solar Heating and Cooling for Buildings and Industry, SHC 2014

Experimental investigation of a liquid desiccant system for air dehumidification working with ionic liquids

Mark T. Zegenhagen[a]*, Cristina Ricart[a], Thomas Meyer[a], Roland Kühn[a], Felix Ziegler[a]

[a]Technische Universitaet Berlin, Institut fuer Energietechnik, Sekretariat KT2, Marchstr. 18, 10587 Berlin, Germany

Abstract

Electrically-driven compression chillers are the commonly used technology for cooling and dehumidifying air. Open sorption systems driven by solar heat are an alternative to conventional air dehumidification technology and may reduce primary energy consumption. For air dehumidification, liquid desiccant systems may exhibit some process engineering and thermodynamic advantages in comparison to solid desiccant systems. The liquid desiccant must exhibit low equilibrium water vapour pressures at the available heat rejection temperature level to achieve low air dew point temperatures and thus a strong air dehumidification with comparably low driving temperatures. Desiccant mass fractions should be as low as possible, but in order to achieve low vapour pressures required desiccant mass fractions may surpass the solubility limit.

In the paper at hand, first experimental results of an internally cooled and heated, open liquid desiccant system working with an ionic liquid designed for air dehumidification are presented. It is demonstrated that ionic liquids designed according to the boundary conditions of the respective application may be a promising alternative to commonly used desiccants such as lithium chloride for solar air dehumidification with comparably high heat rejection and low driving temperatures.

Nomenclature

Roman and greek letters
h   [Jkg^{-1}]   specific enthalpy

---

* Corresponding author. Tel.: +49-314-22933; fax: +49-314-22253.
  E-mail address: zegenhagen@tu-berlin.de

h_E	[Jmol^{-1}]	integral enthalpy of dissolution
h_{vap}	[Jmol^{-1}]	enthalpy of vaporization (water)
L	[Jmol^{-1}]	differential enthalpy of dissolution
$\dot{M}$	[kgh^{-1}]	mass flow rate
p	[Pa]	total pressure
p_v	[Pa]	partial pressure/ equilibrium vapour pressure
R	[Jmol^{-1}K^{-1}]	specific gas constant
T	[K]	absolute temperature
X	[kg$_{IL}$/kg$_{solution}$]	desiccant (salt/ IL) mass fraction in solution
Z	[K]	dew point temperature
α	[-]	boiling line slope in van't Hoff diagram
ω	[kg$_{water}$/kg$_{air}$]	absolute humidity

Subscripts

a	air		r	rich (in water)
A	absorber		S	desiccant solution
amb	ambient		sup	supply air
D	desorber		w	water
ex	exhaust		1	heat rejection temperature level/ inlet/ index
p	poor (in water)		2	driving heat temperature level/ outlet/ index

1. Introduction

The required cooling capacity for cooling air below its dew point consists of sensible heat and latent heat of condensation or even desublimation. An air stream of a temperature of 30°C and a relative humidity of 75% for instance requires a cooling demand consisting of 40% sensible heat and 60% latent heat in order to be cooled down to 10°C and 100% relative humidity. To separate the amount of latent heat needed for the air cooling thus bears a potential for reducing primary energy consumption. Open sorption systems can dehumidify the air and require heat as driving energy; thus they can be driven by thermal solar energy.

Air moisture is ab- or adsorbed in open sorption systems in direct contact with a desiccant at temperatures above the dew point temperature in contrast to conventional vapor compression or absorption chillers which provide the cooling at a certain dew point temperature level. The sensible cooling may then be achieved in a consecutive step after the dehumidification. Open sorption systems consist either of adiabatic or internally cooled dehumidifiers and internally heated regenerators. The internally cooled and/ or heated systems like the one presented in the paper at hand are found to be more efficient [1,2,3].

Liquid desiccants permit a heat recovery between concentrated and diluted desiccant solution as they can be pumped, in contrast to solid desiccants. Inorganic desiccants are commonly preferred over organic desiccants as their loss is negligible due to their comparably low volatility [4,5,6]. Lithium chloride is most commonly used in open liquid sorption systems since it exhibits favorable equilibrium water vapor pressures for air dehumidification [7,8,9]. However, lithium chloride is corrosive and usually crystallizes at large vapor pressure depression, i.e. for low dew point temperatures.

Alternative substances such as ionic liquids are investigated to solve the mentioned problems. Ionic liquids do usually not corrode stainless steel [10]. Besides, ionic liquids may be designed to meet specific system requirements in terms of achievable dew point temperatures at comparatively low driving temperatures which cannot be met by lithium chloride. Ionic liquids may thus be an alternative to be used for solar-driven air dehumidification.

2. System and process description

Fig. 1 depicts a simplified scheme of an internally cooled and heated, open liquid desiccant system for air dehumidification (top), illustrates the described sorption process in a qualitative van't Hoff diagram (bottom, left),

and shows a qualitative diagram of the integral molar enthalpy of dissolution h_E over the desiccant mass fraction X of a binary mixture (bottom, right).
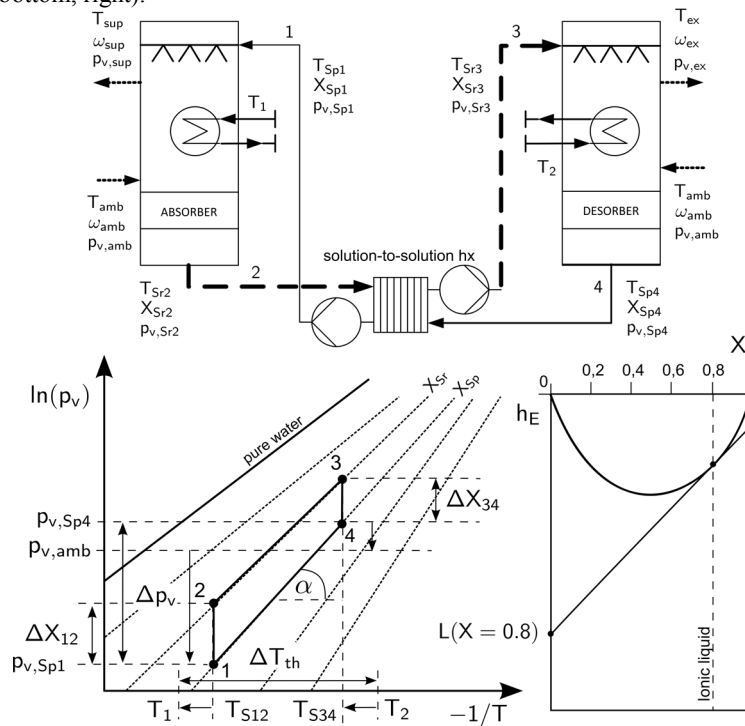

Fig. 1: (top) Example of a simplified scheme of a liquid desiccant system for air dehumidification (dashed thick lines indicate the rich solution; solid thin lines indicate the poor solution; thin dotted lines indicate the air flow); (bottom) Sorption process in a qualitative van't Hoff diagram and a qualitative diagram of the integral molar enthalpy of dissolution h_E as a function of the desiccant mass fraction X of a binary mixture

The system consists of three major components: an absorber, a desorber and a solution-to-solution heat exchanger. In addition, there are two solution pumps for circulating the rich and the poor solution.

The absorber consists of a falling film heat exchanger upon which the solution poor in water (T_{Sp1}, X_{Sp1}, $p_{v,Sp1}$) is trickled. Ambient air (T_{amb}, ω_{amb}, $p_{v,amb}$) is conducted in counter-current flow to the trickling solution film. The ambient air stream is dehumidified as water vapour from the air is taken up by the poor solution X_{Sp1} which is diluted to the desiccant mass fraction X_{Sr2} ($1 \rightarrow 2$). The absorber approximately operates in isothermal mode as the heat of absorption is rejected to a cooling water circuit (at T_1) maintaining the driving force of the mass transfer, i.e. the partial pressure difference in the absorber, as high as possible for the given cooling water temperature level. The dehumidified air stream leaving the absorber (T_{sup}, ω_{sup}, $p_{v,sup}$), which ideally remains at the inlet temperature T_{amb}, can be cooled in a consecutive process step before being conducted to the air-conditioned space as supply air.

In the desorber, the diluted solution X_{Sr2} is heated up in the solution heat exchanger ($2 \rightarrow 3$) to X_{Sr3} by the solution coming from the desorber. The heated rich solution (T_{Sr3}, X_{Sr3}, $p_{v,Sr3}$) is trickled upon the falling film heat exchanger of the desorber where water desorbs from the solution and is taken up by a counter-current flow ambient air stream (T_{amb}, ω_{amb}, $p_{v,amb}$), as the solution is heated during desorption by a hot water circuit of the temperature T_2 ($3 \rightarrow 4$). The regenerated solution X_{Sr4} is cooled down in a consecutive step in the solution heat exchanger ($4 \rightarrow 1$). The humidified air stream (T_{ex}, ω_{ex}, $p_{v,ex}$) exits the desorber. The cooling water supplied to the absorber is usually generated in a cooling tower and the hot water supplied to the desorber is heated up by waste heat or in a solar collector field.

The boiling lines (X_{Sr}, X_{Sp}) in Fig. 1 (bottom, left) must be steep to decrease the necessary driving temperature T_2 for a given heat rejection temperature T_1 and given driving temperature differences in the ab- and desorber, i.e. to

decrease the temperature thrust $\Delta T_{th}=(T_2-T_1)$ for a given partial pressure difference $\Delta p_v=(p_{v,Sp4}-p_{v,Sp1})$. The slope of the boiling lines α can be approximated by the Clausius-Clapeyron equation and reformulated as follows:

$$\alpha = \frac{d(\ln(p_v))}{d(-1/T)} = \frac{h_{vap}+L}{R} = \frac{h_{vap}+[h_E-(\partial h_E/\partial X)\cdot X]}{R} \tag{1}$$

The differential molar enthalpy of dissolution L is a function of the desiccant mass fraction X, the integral molar enthalpy of dissolution h_E and its derivate $(\partial h_E/\partial X)$ as formulated in Eq. (1). A typical curve of a binary solution is depicted in Fig. 1 (bottom, right) with the integral molar enthalpy of dissolution h_E plotted against the desiccant mass fraction X (X=0 pure water and X=1 pure desiccant). It becomes clear that a high differential molar enthalpy of dissolution L like for instance L(X=0.8) may be achieved for comparably high desiccant mass fractions X at which other experimentally investigated liquid desiccants such as lithium chloride usually crystallize. Due to the restriction of crystallization, ionic liquids designed to meet the system requirements in terms of achievable partial pressure differences Δp_v may qualify for solar-driven air dehumidification because they allow to use comparatively low temperature thrusts ΔT_{th}.

3. Test-rig and system control

Fig. 2 depicts the schematic of the rich and poor solution circuits, the air circuit as well as the cooling and hot water circuits of the test-rig at TU Berlin. The details of the measurement equipment and the data acquisition system are found in Appendix A.
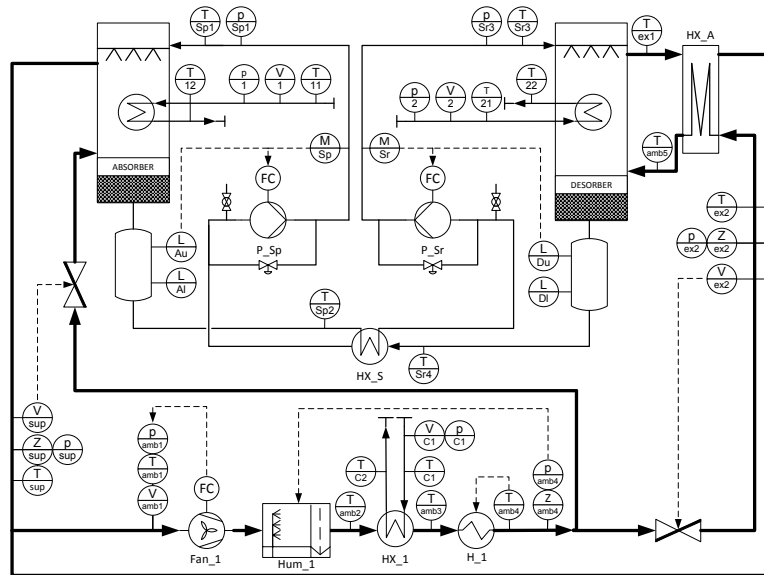

Fig. 2: Schematic of the rich and poor solution circuits, the air circuit as well as the cooling and hot water circuits of the test-rig

The poor and the rich solution mass flow rates measured by Coriolis flow meters (M_{Sp}/ M_{Sr}) are circulated by speed-controlled centrifugal solution pumps (P_{Sp}/ P_{Sr}) in a way that a good wetting is achieved. A safety control overwrites the standard control in case of a signal of one of the upper (L_{Au}/ L_{Du}) or lower (L_{Al}/ L_{Dl}) level sensors indicating an inadmissible solution level in one of the solution reservoirs. The solution levels in the reservoirs are equalized by the safety control maintaining the test-rig in a quasi-steady-state and avoiding the pumps to run dry or the reservoirs to overflow.

The overall air flow rate V_{amb1} is circulated in a closed loop by means of a speed-controlled fan (Fan_1). The closed loop allows to condition the air inlet of the ab- and desorber in terms of temperature and absolute humidity and to maintain steady-state conditions for an extended period of time and reproduce the conditions independent of the actual weather. The volume air flow may be humidified in the humidifier (Hum_1), cooled down to the desired dew point temperature in the consecutive condenser (HX_1) and heated back up again in the electrical heater (H_1). The dew point temperature Z_{amb4} and the inlet temperature of the air flow T_{amb4} are controlled in that manner. The ratio of the air flow rate of the absorber and the desorber (V_{sup}/V_{ex2}) is controlled by blinds in the air ducts.

The volume flow rates of the external hot water circuit V_2 and cooling water circuits V_1 and V_{C1} are controlled by speed-controlled centrifugal pumps (not shown in Fig. 3). The inlet temperature of the hot water circuit T_{21} and the cooling water circuits T_{11} and T_{C1} are controlled by an electrical heater of 25kW nominal capacity or three-way mixing valves, respectively (not shown in Fig. 3).

4. Experimental results and discussion

The steady-state criteria of the experiments and the uncertainty analysis of the experimental results are discussed in Appendix B. On the left side of Fig. 3, the absolute humidity of the air flow at the absorber outlet ω_{sup} over the absolute humidity at the absorber inlet ω_{amb} is shown with with the hot water temperature at the desorber T_2 as a parameter [338.15K (symbol Δ), 348.15K (symbol o), 358.15K (symbol x)]. The corresponding absolute humidity of the air flow at the desorber outlet ω_{ex} over the absolute humidity at the desorber inlet ω_{amb} is depicted on the right hand side of Fig. 3. Therefore, a pair of points (ω_{sup}, ω_{ex}) results from every experimental operation point ω_{amb}. In addition, the best fit straight lines corresponding to the experiments at constant hot water temperature are depicted.
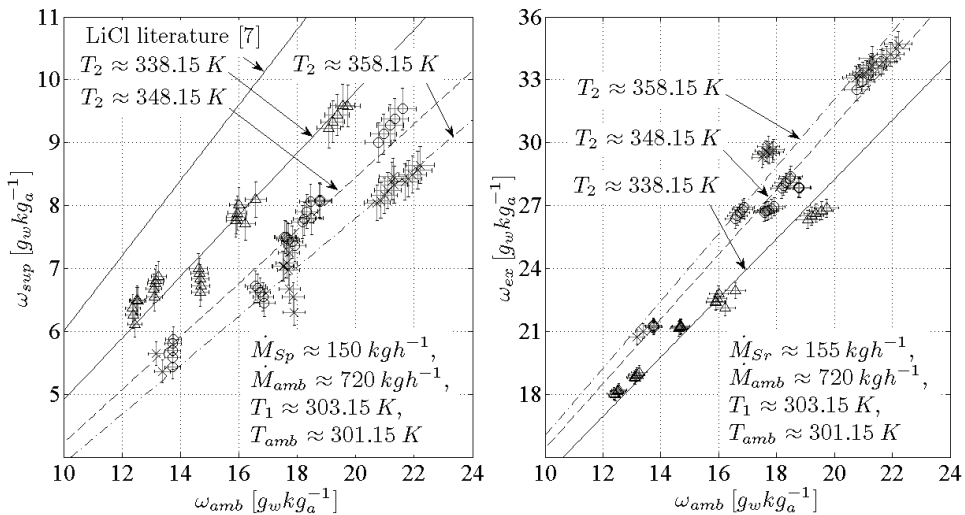

Fig. 3: (left) Absolute humidity of the air flow at the absorber outlet ω_{sup} over the absolute humidity of the absorber inlet ω_{amb}; (right) Corresponding absolute humidity of the air flow at the desorber outlet ω_{ex} over the absolute humidity of the desorber inlet ω_{amb} [parameter T_2: 338.15K (symbol Δ), 348.15K (symbol o), 358.15K (symbol x)] and best fit straight lines

The solution mass flow rates $\dot{M}_{Sp}$ and $\dot{M}_{Sr}$ were set to $150 kgh^{-1}$ and $155 kgh^{-1}$, respectively, and both air mass flow rates at the ab- and desorber $\dot{M}_{amb}$ to $720 kgh^{-1}$ (±15% on average). The air temperature T_{amb} and the cooling water temperature T_1 at the absorber were set to 301.15K and 303.15K, respectively.

The absolute humidity of the air flow at the absorber outlet ω_{sup} on the left hand side in Fig. 3 ranges from about $9.8 g_w kg_a^{-1}$ to $5.4 g_w kg_a^{-1}$ for a corresponding absolute humidity at the absorber inlet ω_{amb} from about $22.1 g_w kg_a^{-1}$ to $12.1 g_w kg_a^{-1}$. The absolute humidity of the air flow at the desorber outlet ω_{ex} on the right hand side in Fig. 3

ranges from about $34.7 g_w kg_a^{-1}$ to $18 g_w kg_a^{-1}$ for the corresponding absolute inlet humidity. The absolute humidity at the absorber outlet ω_{sup} and the desorber outlet ω_{ex} increase with increasing absolute humidity ω_{amb} as expected.

The respective increase is in rough approximation linear as it becomes evident in the straight lines fitted to the experimental results at constant hot water temperature. The linearity is due to the fact that the driving partial water vapor pressure differences in the ab- and desorber change for a constant driving and heat rejection temperature in rough approximation linearly with the desiccant mass fractions while the mass transfer coefficients and effective area remain constant in the investigated operation range. The dehumidification at the absorber and the humidification at the desorber are thus a nearly linear function of the absolute inlet humidity and the resulting desiccant mass fractions only.

The higher the desorber inlet temperature T_2 in the experiments is, the more the air flow is dehumidified for a given absolute humidity ω_{amb} which becomes evident in Fig. 3 (left) in particular for high values of the absolute humidity ω_{amb}. In comparison to experiments with LiCl reported in literature [7] which are shown in Fig. 3 (left) in the straight line, the absolute humidity is low at a comparably high heat rejection temperature T_1 of 30°C and the given temperature thrusts ΔT_{th}. The increase in dehumidification with the increasing hot water temperature at the desorber T_2 decreases in Fig. 3 for a given absolute inlet humidity ω_{amb} as the driving partial water vapor pressure differences decrease with increasing desiccant mass fractions.

The experiments in Fig. 3 have been conducted with a constant cooling water inlet temperature T_1 and with constant solution mass flow rates $\dot{M}_S$. Now, in another set of experiments, these values have been varied. Fig. 4 shows the absolute humidity of the air, i.e. ω_{ex}, ω_{amb} and ω_{sup}, over the cooling water inlet temperature T_1 with a constant solution flow rate $\dot{M}_S$ of $150 kgh^{-1}$ on the left hand side and over the solution mass flow rates $\dot{M}_{Sp}$ and $\dot{M}_{Sr}$ with a constant cooling water inlet temperature T_1 on the right hand side.
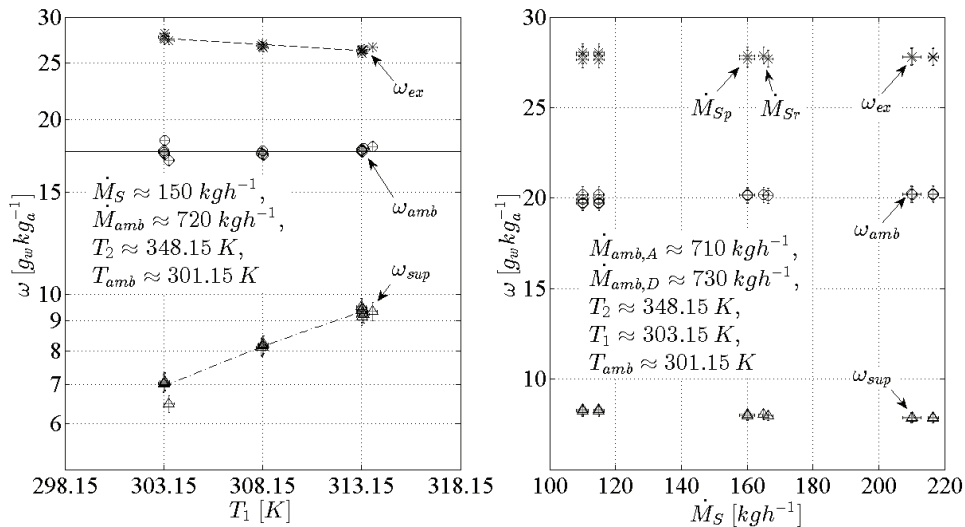

Fig. 4: (left) Absolute humidity of the air flow at the desorber outlet ω_{ex} (symbol x), at the ab- and desorber inlet ω_{amb} (symbol o), and at the absorber outlet ω_{sup} (symbol Δ) over the cooling water inlet temperature at the absorber T_1; (right) Humidity over the solution mass flow $\dot{M}_S$

The hot water temperature T_2 has in all cases been set to 348.15K. The cooling water temperature T_1 at the absorber has been varied between 303.15K and 313.15K in the experiments presented on the left hand side of Fig. 4 and the solution mass flow rates $\dot{M}_S$ have been varied from $105 kgh^{-1}$ to $215 kgh^{-1}$ in the experiments presented on the right hand side. The solution mass flow rates $\dot{M}_{Sp}$ and $\dot{M}_{Sr}$ slightly differ in the experiments due to the difference in water content, as it becomes clear on the right hand side.

The absolute humidity of the air flow at the outlet of the absorber ω_{sup} increases from about $7 g_w kg_a^{-1}$ to $9.5 g_w kg_a^{-1}$ for a constant inlet humidity ω_{amb} of about $17.5 g_w kg_a^{-1}$ with a cooling water inlet temperature T_1 increasing from 303.15K to 313.15K. The dehumidification reduces by 14% ($2.5/17.5 g_w kg_a^{-1}$) as the driving

partial pressure difference at the absorber decreases ceteris paribus with an increasing cooling water inlet temperature T_1. The absolute humidity of the air flow at the outlet of the desorber ω_{ex} decreases accordingly.

It becomes clear in Fig. 4 in the variation of the solution mass flow rates on the right hand side that there is no noticeable influence on the dehumidification for the given operating conditions. Therefore, the salt mass fraction differences ΔX_{12} and ΔX_{34} from Fig. 1 (not measured) must have been negligible in the experiments. The solution mass flow rates in the experiments from Fig. 3 have been chosen visually for a good wetting of the heat exchangers. They can be reduced further without a decrease in dehumidification in order to reduce parasitic consumptions.

5. Conclusion

An open sorption system working with an ionic liquid designed for air dehumidification has been successfully operated at comparably high absolute heat rejection temperatures and low temperature thrusts. The dehumidification potential for driving temperatures between 338.15K and 358.15 and heat rejection temperatures of up to 313.15K seems promising in comparison to experiments with lithium chloride reported in literature. Ionic liquids can therefore be an interesting alternative for solar air-conditioning, if long-term system operation is demonstrated.

Acknowledgements

Appendix A. Measurement and data acquisition system

The temperature sensors used in the test-rig from Fig. 3 are all Pt100 resistance thermometers (screw-in sensors in solution and water circuits, averaging value temperature sensors in the air). Absolute pressure transducers are employed. The volumetric flow is measured by MID flow meters in the water circuits and by pitot tubes in a bar grate in the air. The solution mass flow rates are determined by Coriolis flow meters. The dew point temperature is measured with dew point temperature sensors. Tab. 1 lists the sensors, the measurement range and the errors.

Table A.1. Sensors, measurement ranges, sensor errors and terminal errors.

Sensor	Sensor range	Sensor error f	Terminal error f (gain error, offset error)
T_{11}/ T_{12}/ T_{21}/ T_{22}/ T_{Sp1}/ T_{Sp2}/ T_{Sr3}/ T_{Sr4}	$73.15 \ldots 1123.15K$	$\pm(0.15K + 0.02\,|T_i|)$	$\pm0.09K$
T_{sup}/ T_{amb1}/ T_{amb2}/ T_{amb3}/ T_{amb4}/ T_{amb5}/ T_{ex1}/ T_{ex2}	$73.15 \ldots 1123.15K$	$\pm(0.3K + 0.05\,|T_i|)$	$\pm0.09K$
p_{Sr1}/ p_{Sp3}	$10^5 \ldots 3 \cdot 10^5 Pa$	$\pm 2000\ Pa$	$\pm(0.0076 \cdot p_i + 570Pa), \pm165Pa$
p_1/ p_2/ p_{c1}	$10^5 \ldots 4 \cdot 10^5 Pa$	$\pm 1500\ Pa$	$\pm(0.0076 \cdot p_i + 760Pa), \pm220Pa$
P_{sup}/ p_{amb1}/ p_{amb4}/ p_{ex2}	$8 \cdot 10^4 \ldots 1.2 \cdot 10^5 Pa$	$\pm 420Pa$	$\pm(0.0076 \cdot p_i - 532\ Pa), \pm22Pa$
V_1, V_2/ V_{C1}	$0 \ldots 6 m^3 h^{-1}/$ $0 \ldots 2.5 m^3 h^{-1}$	$\pm(0.003 \cdot \dot{V}_i$ $+ 0.0036 m^3 h^{-1})$ $\pm (0.003 \cdot V_i$ $+ 0.0013 m^3 h^{-1})$	$\pm(0.0076 \cdot V_i + 0.0114 m^3 h^{-1}),$ $\pm0.0033 m^3 h^{-1}/$ $\pm(0.0076 \cdot V_i + 0,0048 m^3 h^{-1})$ $\pm0.0014 m^3 h^{-1}$
V_{sup}, V_{ex2}/ V_{amb1}	$0 \ldots 30 Pa/ 0 \ldots 100 Pa$	$\pm 0.06\ /0.2 Pa$	$\pm(0.0087 \cdot p_i + 0.0653\ Pa),\ \pm0.021 Pa/$ $\pm(0.0087 \cdot p_i + 0.1087\ Pa), \pm0.034 Pa$
M_{Sr}, M_{Sp}	$100 kg h^{-1} \ldots 400 kg h^{-1}$	$\pm 0.001 \cdot M_i\ kg/h$	$\pm(0.0087 \cdot M_i + 0.6101 kg/h),$ $\pm0.193 kg/h$
Z_{amb4}/ Z_{sup}/ Z_{ex2}	$278.15 \ldots 303.15K/$ $248.15 \ldots 298.15K/$ $293.15 \ldots 318.15K$	$\pm0.2\ K$	$\pm(0.0076 \cdot Z_i + 0.0855K), \pm 0.014K$ $\pm(0.0076 \cdot Z_i - 0.285\ K), \pm0.028K$ $\pm(0.0076 \cdot Z_i + 0.1045K), \pm0.0138K$

All measurement signals were recorded in intervals of 3s.

Appendix B. Uncertainty analysis

The experiments must be conducted under steady state conditions to avoid transient effects or trends. The start-up time for the experiments has been about 2h to 3h. Tab. 2 lists the steady-state criteria for the set-values which must be met during a period of 10min, i.e. 200 measurements, to be used for determining a steady-state average value.

Table B.2. Steady-state criteria.

Sensor	Steady-state criteria
$\Delta T\_1/ \Delta T\_2/ \Delta T\_amb4/ \Delta T\_Sp1/ \Delta T\_Sr3$	$< \pm 0.3$ K
$\Delta V\_amb1/ \Delta V\_1/ \Delta V\_2$	$< \pm 5\%$
$\Delta M\_Sr/ \Delta M\_Sp$	$< \pm 5\%$
ΔZ_amb4	$< \pm 0.3$K

The steady-state conditions were usually maintained during 1.5h to 2h. The methodology to analyze the statistical processes which are superimposed on the deterministic processes of the experiments is as follows. The empirical average of a finite sample n of a normally distributed physical quantity x (like the temperatures, the pressures etc.) is calculated by its arithmetic average and its sample standard deviation is estimated as follows:

$$\bar{x}_n = \frac{1}{n} \cdot \sum_{i=1}^{n} x_i, \qquad s_n^2 = \frac{1}{(n-1)} \cdot \sum_{i=1}^{n} (\bar{x}_n - x_i)^2 \tag{B.1}$$

The deviation margin $U_{\bar{x}_n}$ of the directly measured physical quantity x and the deviation margin U_y of a physical quantity y (like the absolute humidity etc.) which is calculated from other independent directly measured physical quantities $x_1, x_2 \ldots x_k$ are determined as:

$$U_{\bar{x}_n} = 2 \cdot \sqrt{s_n^2 + \sum_{j=1}^{m} s_{R,j}^2}, \qquad s_R = f/\sqrt{3}, \qquad U_y^2 = \sum_{l=1}^{k} \left(\partial y / \partial x_l \cdot U_{\bar{x}_n} \right) \tag{B.2}$$

The standard deviation of the rectangular distribution is s_R which results from the errors of the measurement sensors and the data acquisition system f_i from Tab. A.1. The standard deviation s_n^2 results from each individual experiment.

References

[1] Luo Y, Yang H, Lu L, Qi R. A review of the mathematical models for predicting the heat and mass transfer process in the liquid desiccant dehumidifier. *Renew Sust Energ Rev* 2014;31:587-599.
[2] Yin Y, Zhang X. Comparative study on internally heated and adiabatic regenerators in liquid desiccant air conditioning system. *Build Environ* 2010;45:1799-1807.
[3] Liu XH, Chang XM, Xia JJ, Jiang Y. Performance analysis on the internally cooled dehumidifier using liquid desiccant. *Build Environ* 2009; 44:299-308.
[4] Jain S, Bansal PK. Performance analysis of liquid desiccant dehumidification systems. *Int J Refrig* 2011;36:1180-1186.
[5] Tsai C, Soriano A, Li M. Vapor pressures, densities and viscosities of the aqueous solutions containing (triethylene glycol or propylene glycol) and (LiCL or LiBr). *J Chem Thermodyn* 2009;41:623-631.
[6] Liu XH, Yi XQ, Jang Y. Mass transfer performance comparison of two commonly used liquid desiccants: LiBr and LiCl aqueous solutions. *Energ Convers Manage* 2011;51:180-190.
[7] Gommed K, Grossman G. Experimental investigation of a liquid desiccant system for solar cooling and dehumidification. *Sol Energy* 2007;81:131-138.
[8] Gandhidasan P. A simplified model for air dehumidification with liquid desiccant. *Sol Energy* 2004;76:409-416.
[9] Luo Y, Shao S, Xu H, Tian C, Yang H. Experimental and theoretical research of a fin-tube type internally-cooled liquid desiccant dehumidifier. *Appl Energ* 2014;133:127-134.
[10] Perissi I, Bardi U, Caporali S, Lavacchi A, High temperature corrosion properties of ionic liquids. *Corros Sci* 2006;48:2349-2362.